

Fermion WIMPless Dark Matter at DeepCore and IceCube

Vernon Barger¹, Jason Kumar², Danny Marfatia³ and Enrico Maria Sessolo³

¹*Department of Physics, University of Wisconsin, Madison, WI 53706, U.S.A.*

²*Department of Physics and Astronomy, University of Hawai'i, Honolulu, HI 96822, U.S.A.*

³*Department of Physics and Astronomy, University of Kansas, Lawrence, KS 66045, U.S.A.*

Abstract

We investigate the prospects for indirect detection of fermion WIMPless dark matter at the neutrino telescopes IceCube and DeepCore. The dark matter annihilating in the Sun is a hidden sector Majorana fermion that couples through Yukawa couplings to a connector particle and a visible sector particle, and it exhibits only spin-dependent scattering with nuclei via couplings to first generation quarks. We consider cases where the annihilation products are taus, staus, or sneutrinos of the three generations. To evaluate the muon fluxes incident at the detector, we propagate the neutrino spectra through the solar medium and to the Earth and account for the effects of neutrino oscillations, energy losses due to neutral- and charged-current interactions, and tau regeneration. We find that for the stau and sneutrino channels, a 5 yr 3σ detection of dark matter lighter than about 300 GeV is possible at IceCube for large Yukawa couplings or for dark matter and connector particles with similar masses. The tau channel offers far better detection prospects. However, due to its lower energy threshold and better muon background rejection capability, DeepCore is able to detect signals in all annihilation channels and for a wider range of dark matter masses.

1 Introduction

There has long been interest in the use of neutrino experiments for indirect dark matter (DM) detection, with a particular focus on neutrino signals from DM annihilation in the Sun. The basic idea is that DM particles can be captured by the Sun if they lose sufficient kinetic energy through elastic scattering from solar nuclei. This leads to an enhanced DM number density in the solar core, where DM can annihilate to standard model (SM) products. These products in turn decay, producing a neutrino flux which can be detected by Earth-based detectors. Because the Sun is (for most models under consideration) in equilibrium, the DM capture rate is equal to twice the annihilation rate. Thus, the neutrino flux on Earth is determined by the capture rate, which in turn is determined (up to a few $\mathcal{O}(1)$ factors related to solar physics) by the DM mass m_χ and the DM-nucleon scattering cross section σ . This is one of the key advantages of neutrino-based indirect searches for DM: the event rate is directly related to the scattering cross section, without many of the astrophysical uncertainties which attend other indirect detection strategies. Moreover, it is in principle possible to directly compare search results at neutrino experiments with those at direct-detection experiments, which also measure the DM-nucleon scattering cross section; for a recent discussion, see [1]. This allows one to corroborate a signal at one type of experiment with a signal at a very different type of experiment, which is desirable.

The downside, however, is that for much of the (m_χ, σ) -parameter space, sensitivities for current and future neutrino detectors have already been surpassed by direct-detection bounds, implying that neutrino detectors may have difficulty providing new input to DM studies. However, there are two scenarios where neutrino experiments are expected to shine. One is at low-mass ($m_\chi \sim 4 - 10$ GeV). In this mass range, bounds from direct-detection experiments tend to become significantly worse because the nuclear recoil energies often fall below the experimental threshold. Experiments such as Super-Kamiokande (Super-K) and other proposed water Cherenkov or liquid scintillator-type detectors can provide the best bounds in this range [2], and could be sensitive to spin-independent (SI) scattering cross sections $\sigma_{SI} \sim 10^{-5}$ pb. DM in this range can potentially explain the annual modulation signal seen by the DAMA experiment ([3], though see also [4]), as well as unexplained events recently reported by the CDMS and CoGeNT Collaborations [5, 6, 7]. There is thus considerable interest to cross-check these results with neutrino detectors.

Another scenario for which neutrino experiments can excel is for models where the DM-nucleon scattering is largely spin-dependent (SD), rather than SI [8]. The reason is that DM can then be captured by SD scattering from hydrogen in the Sun, leading to significant neutrino fluxes. Current direct-detection experiments provide much less sensitivity to SD scattering and the best bounds are set by indirect detection experiments, even at large m_χ . This has been the focus of large neutrino detectors, such as AMANDA or IceCube. For example, with 1800 live days of running, IceCube

could be sensitive to $\mathcal{O}(100 \text{ GeV})$ DM with $\sigma_{SD} \sim 10^{-5} \text{ pb}$ [9]. Although the relatively high threshold energy of these detectors limits their utility in studying the low-mass DM, their large size makes them ideal for studying higher-mass DM ($m_\chi \geq 100 \text{ GeV}$) with $\sigma_{SD} \gg \sigma_{SI}$.

Direct detection is much more sensitive to σ_{SI} due to the possibility of coherent scattering in the nucleus. Direct-detection experiments, including CDMS and XENON100, currently have a sensitivity to σ_{SI} in the $\mathcal{O}(100 \text{ GeV})$ mass range of about 3 orders of magnitude [5, 10] greater than the IceCube projected 1800 d sensitivity to σ_{SD} . But for models with $\sigma_{SI} \ll \sigma_{SD}$, complementary coverage from neutrino detectors becomes important. This complementary coverage is especially important if one goes beyond models of weakly interacting massive particles (WIMPs). The recently proposed WIMPlless model of dark matter [11, 12] is notable because it provides a very generic hidden sector DM candidate which naturally has about the right relic density to match astronomical observations, regardless of the mass of the DM particle or the details of the hidden sector. This versatility suggests the possibility of specific WIMPlless models with almost exclusively SD scattering, for which the best detection prospects would lie at neutrino detectors.

We present a model of WIMPlless dark matter where the DM candidate is a Majorana fermion in the hidden sector. At tree level, it will exhibit only SD scattering with SM nuclei. We find that significant neutrino fluxes on Earth arise from models where DM annihilates either to tau, stau, or sneutrino pairs. We consider the detection prospects for this type of model at DeepCore and IceCube.

The paper is organized as follows: In Sec. 2, we review WIMPlless dark matter and describe the properties of the fermion candidate DM particle. In Sec. 3, we obtain the neutrino spectra arising from the decay of various annihilation products. In Sec. 4, we discuss the predicted event rates at DeepCore and IceCube, and we present our conclusions in Sec. 5.

2 WIMPlless Dark Matter

Here we briefly review the WIMPlless DM scenario [11]. This scenario is closely related to gauge-mediated supersymmetry breaking (GMSB) [13]. Our theory consists of a supersymmetry (SUSY)-breaking sector, the visible minimal supersymmetric standard model (MSSM) sector and a hidden sector, plus a *connector* sector which we introduce in the next subsection. We assume there is at least one chiral superfield S in the SUSY-breaking sector, and there are messenger fields Φ , $\bar{\Phi}$ between the SUSY-breaking and MSSM sectors and Φ_χ , $\bar{\Phi}_\chi$ between the SUSY-breaking and hidden sector. S is coupled to the messenger fields through Yukawa couplings in the superpotential $W = \lambda \bar{\Phi} S \Phi + \lambda_\chi \bar{\Phi}_\chi S \Phi_\chi$. The effect of GMSB on the MSSM sector is well-known: the chiral field S acquires a vacuum expectation value $\langle S \rangle = M + \theta^2 F$. The Yukawa couplings generate messenger mass terms of order $m_{mess} \sim \lambda M$ and messenger mass splittings of order $F_{mess} = \lambda F$.

Once the heavy gauge messengers are integrated out, the low-energy effective theory has a new SUSY-breaking soft scale m_{soft} which is generated by diagrams with the messengers running in the loops,

$$m_{soft} \sim \frac{g^2}{(4\pi)^2} \left(\frac{F_{mess}}{m_{mess}} \right) = \frac{g^2}{(4\pi)^2} \frac{F}{M}, \quad (1)$$

where g is the largest relevant gauge coupling. The effect in the hidden sector is qualitatively the same, and we assume that some unbroken symmetry stabilizes a particle in the hidden sector at the soft SUSY-breaking scale, whatever it may be. The soft SUSY-breaking scale in the hidden sector is then given by

$$m_\chi \sim \frac{g_\chi^2}{(4\pi)^2} \left(\frac{F_{mess\chi}}{m_{mess\chi}} \right) = \frac{g_\chi^2}{(4\pi)^2} \frac{F}{M}, \quad (2)$$

where $F_{mess\chi} = \lambda_\chi F$ and $m_{mess\chi} \sim \lambda_\chi M$. Because the ratio F/M is determined by the dynamics of the SUSY-breaking sector, it appears in the same way in the soft scale in both the hidden sector and MSSM sector. We thus find

$$\frac{g_\chi^4}{m_\chi^2} \sim \frac{g^4}{m_{soft}^2} \propto \left(\frac{M}{F} \right)^2. \quad (3)$$

The ratio g^4/m^2 sets the annihilation cross section for a particle of mass of order m through gauge interactions of strength g , and the cross section in turn determines the thermal relic density, ($\Omega \propto \langle \sigma v \rangle^{-1}$ [14]). To obtain a thermal relic density which matches astronomical observations, a DM candidate would need an annihilation cross section $\langle \sigma v \rangle \sim 1$ pb. The ‘‘WIMP miracle’’ is the amazing fact that, when calculated at the electroweak scale, the ratio g_{weak}^4/m_{weak}^2 yields an annihilation cross section which is in fact close to 1 pb. But we see from Eq. (3) that the annihilation cross section for a stable particle at the hidden sector soft SUSY-breaking scale will be approximately the same; this DM candidate will thus automatically have approximately the right relic density. Most importantly, the scale m_χ of the DM is a free parameter, thus motivating DM searches over a wide range of masses.

2.1 Fermionic Model

In the WIMPlless scenario, DM is stabilized by a hidden sector symmetry (which may be discrete). We let $\hat{X}_{L,R}$ be chiral supermultiplets in the hidden sector, with a fermionic mass eigenstate of $X_{L,R}$ (henceforth denoted as X) being the lightest particle charged under the stabilizing symmetry. WIMPlless DM interacts with the SM through Yukawa couplings, which permit the exchange of exotic ‘‘connector’’ particles. Consider the interaction superpotential,

$$\begin{aligned} W = & \lambda_{Li} \hat{X}_L \hat{Y}_L \hat{Q}_{Li} + \lambda_{Ri} \hat{X}_R \hat{Y}_R \hat{Q}_{Ri} + m_Y \hat{Y}_L \hat{Y}_R \\ & + \lambda'_{Lj} \hat{X}_L \hat{Y}_L^{lep} \hat{L}_{Lj} + \lambda'_{Rj} \hat{X}_R \hat{Y}_R^{lep} \hat{L}_{Rj} + m_{Y^{lep}} \hat{Y}_L^{lep} \hat{Y}_R^{lep}, \end{aligned} \quad (4)$$

where $\hat{Q}_{Li,Ri}$ are MSSM chiral quark multiplets, $\hat{L}_{Li,Ri}$ are MSSM chiral lepton multiplets, and $\hat{Y}_{L,R}$ and $\hat{Y}_{L,R}^{lep.}$ are the exotic connector particles which are charged under both the MSSM and the hidden sector symmetry. Gauge-invariance requires the $\hat{Y}_{L,R}$ to be chiral under the MSSM, so their fermion components behave like exotic fourth generation quarks (similarly, the fermions of $\hat{Y}_{L,R}^{lep.}$ are exotic fourth generation leptons). The mass terms $m_Y, m_{Y^{lep.}}$ are thus set by electroweak symmetry breaking, and are determined by the Higgs vacuum expectation value and Yukawa couplings.

The mass of the exotic quarks is constrained by perturbativity and precision electroweak data to the range $m_Y \lesssim 600 \text{ GeV}$ [15, 16, 17]. Since the DM particle X is the lightest particle charged under the stabilizing hidden sector symmetry, it is constrained to be lighter than any of the exotic connectors.

Since the exotic squarks $\tilde{Y}_{L,R}$ can get mass terms which are decoupled from electroweak symmetry breaking, there is no relevant upper bound on $m_{\tilde{Y}_{L,R}}$. But $m_{\tilde{Y}_{L,R}}$ can be bounded from below by direct searches at colliders. The exotic squarks can be pair produced through QCD processes, with each decaying via $\tilde{Y}_{L,R} \rightarrow X + u, d$. The signal at a hadron collider would be exclusive dijet production with missing transverse energy, which is the same signature as that of leptoquark pair production, with decay to a quark and neutrino. A CDF Collaboration search for this signature [18] places a bound on the leptoquark mass at $m_{LQ} > 187 \text{ GeV}$. Since, in our case, the missing energy arises from a relatively heavy-DM particle X (as opposed to a nearly massless neutrino), the lower bound on the mass of the exotic squark will be even weaker, and for our analysis it will not be constraining.

The DM candidate X can be either a Dirac or Majorana fermion. We thus see that DM-nucleon scattering can arise from s - or u -channel exchange of the Y multiplets, as represented in Fig. 1. After a Fierz transformation, we can write the DM-parton scattering matrix element in terms of

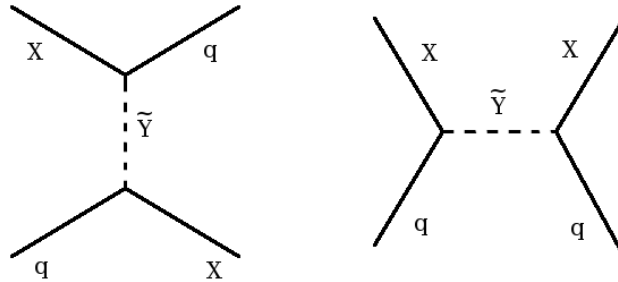


Figure 1: The u - and s -channel Feynman diagrams for Xq scattering.

an effective operator,

$$\mathcal{O} = \frac{\lambda_{Li}^2}{2(m_X^2 - m_{Y_L}^2)^2} (\bar{q}_i \gamma^\mu P_L q_i) (\bar{X} \gamma_\mu P_R X) + \frac{\lambda_{Ri}^2}{2(m_X^2 - m_{Y_R}^2)^2} (\bar{q}_i \gamma^\mu P_R q_i) (\bar{X} \gamma_\mu P_L X). \quad (5)$$

We assume from here on that the scalars from the Y_L and Y_R multiplets have degenerate mass; $m_{\tilde{Y}_L} = m_{\tilde{Y}_R} = m_{\tilde{Y}}$. If we only retain terms which provide a velocity-independent contribution to DM-nucleon scattering, we can write this operator as

$$\mathcal{O} \approx \frac{\lambda_{Li}^2 + \lambda_{Ri}^2}{8(m_{\tilde{Y}}^2 - m_X^2)} [(\bar{q}_i \gamma^\mu \gamma_5 q_i) (\bar{X} \gamma_\mu \gamma_5 X) - (\bar{q}_i \gamma^\mu q_i) (\bar{X} \gamma_\mu X)]. \quad (6)$$

We find that if X is a Dirac fermion, then

$$\begin{aligned} \sigma_{SI} &= \frac{1}{4} \frac{m_r^2}{64\pi(m_{\tilde{Y}}^2 - m_X^2)^2} \left[\sum_i (\lambda_{Li}^2 + \lambda_{Ri}^2) (Z B_i^p + (A - Z) B_i^n) \right]^2 \\ \sigma_{SD} &= \frac{1}{4} \frac{m_r^2}{4\pi(m_{\tilde{Y}}^2 - m_X^2)^2} \frac{J+1}{J} \left[\sum_i (\lambda_{Li}^2 + \lambda_{Ri}^2) (\langle S_p \rangle \Delta_i^{(p)} + \langle S_n \rangle \Delta_i^{(n)}) \right]^2, \end{aligned} \quad (7)$$

where the 1/4 factor accounts for the fact that the DM is not its own antiparticle, so only the s - or u -channel will contribute to $Xq \rightarrow Xq$ scattering. $m_r = m_X M_N / (m_X + M_N)$ is the reduced mass of the DM-nucleus system. The vector-vector part of the effective operator generates σ_{SI} , while the axial-axial part generates σ_{SD} . The $B_i^{(p,n)}$ parametrize the quark content of the nucleon, and the $\Delta_i^{(p,n)}$ its quark spin content. The $\langle S_{p(n)} \rangle$ are the expectation values of the spin content of the proton (neutron) group in the nucleus. The numerical values of Δ_i^p corresponding to structure functions including next-to-next-to-leading order QCD corrections are [19],

$$\Delta_u^p = 0.78 \pm 0.02, \quad \Delta_d^p = -0.48 \pm 0.02, \quad \Delta_s^p = -0.15 \pm 0.02. \quad (8)$$

As noted in Ref. [20], uncertainties in quark spin contents can lead to substantial variations in σ_{SD} .

If the DM is Dirac, then a σ_{SD} which is potentially detectable at DeepCore would already be ruled out by direct-detection constraints on σ_{SI} . We therefore focus on the case where X is a Majorana fermion which is stabilized by a Z_2 symmetry (so $CXC = X$). The vector-vector part of the effective operator is then identically zero and the scattering cross section is necessarily SD ($\sigma_{SI} = 0$), and we find

$$\sigma_{SD} = \frac{m_r^2}{4\pi(m_{\tilde{Y}}^2 - m_X^2)^2} \frac{J+1}{J} \left[\sum_i (\lambda_{Li}^2 + \lambda_{Ri}^2) (\langle S_p \rangle \Delta_i^{(p)} + \langle S_n \rangle \Delta_i^{(n)}) \right]^2, \quad (9)$$

since now both s and u channels contribute. Note that we have only included the velocity-independent terms, and only at tree level. Since the bounds on σ_{SI} are ~ 4 orders of magnitude stronger than the expected IceCube bounds on σ_{SD} , one might wonder if this model could be probed

by direct-detection experiments via velocity-dependent or loop-induced spin-independent effective operators. One would expect velocity-dependent operators to be suppressed by at least 10^{-6} . Also, loop-induced SI effective operators would be suppressed by $(\alpha/4\pi)^2 \sim 10^{-6}$. Thus, with further improvements, direct-detection probes of σ_{SI} induced by one-loop diagrams may be comparable to probes of σ_{SD} at tree level by IceCube. This is an interesting subject for future study, but is beyond the scope of the present work.

In our model, DM can have axial-vector couplings to the light and/or the heavy quarks. Scalar DM coupling to heavy quarks was studied in detail in [21], but no such study has been performed in the case of axial-vector coupling. Instead, we consider the case where DM couples to light quarks; if DM couples to more than one quark generation, then there is a potential for dangerous flavor-changing neutral currents. As a simple solution to this constraint, we assume that the only DM-quark coupling is to the first generation. We take $\lambda \equiv \lambda_{Lu} = \lambda_{Ru} = \lambda_{Ld} = \lambda_{Rd}$, and $\lambda_{Ls} = \lambda_{Rs} = 0$.

2.2 Annihilation

In WIMPless DM models, the annihilation cross section to hidden sector particles is naturally $\langle \sigma_{ann.v} \rangle \sim 1$ pb at the time of decoupling. From the form of the Yukawa couplings, we see that DM can also annihilate to MSSM matter multiplets. The annihilation cross section to MSSM particles should not be very much larger than 1 pb, or else annihilation will dilute the relic density and ruin the WIMPless miracle. But in order to get a significant flux at neutrino detectors, it is necessary for the annihilation branching fraction to MSSM particles to be comparable to unity.

Since we are considering the case where the DM is Majorana, annihilation to light fermions is chirality/ p -wave suppressed. Also, in order to obtain SD scattering without inducing dangerous flavor-changing neutral currents, we assume that the only quark multiplets which the DM couples to are the first generation multiplets. So DM annihilation to quarks will be suppressed; if the DM annihilation to the hidden sector is not suppressed at current times, then the branching fraction for DM in the Sun to annihilate to quarks will be very small. One caveat to this statement is that if the light hidden sector particles are also fermions, then annihilation to the hidden sector is also chirality/ p -wave suppressed. This does not significantly suppress the annihilation cross section at decoupling, but may suppress the annihilation cross section to hidden sector particles in the Sun by enough to allow the branching fraction to quarks to be sizable. In this case, DM annihilation to quarks in the Sun can be a significant source of neutrinos observed at IceCube. But if there are light vectors or scalars (perhaps Goldstone bosons) in the hidden sector, then annihilation to these products is not suppressed, and the cross section for hidden sector annihilation would be expected to be ~ 1 pb. To get an annihilation cross section to SM particles of comparable magnitude, one

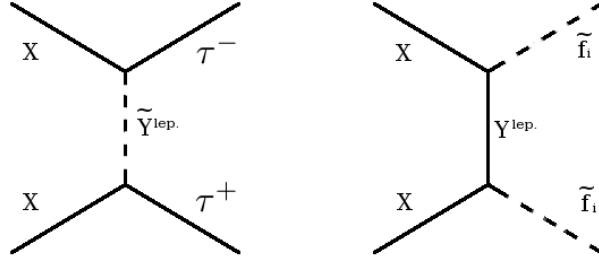


Figure 2: Feynman diagrams for DM annihilation into $\tau^-\tau^+$ and into $\tilde{f}_i\tilde{f}_i^*$.

must either consider squark final states, or make use of Yukawa couplings to SM leptons. Then, the only relevant MSSM annihilation products are τ , $\tilde{l}_{L,R}$ and the first generation squarks $\tilde{u}_{L,R}$ and $\tilde{d}_{L,R}$. These annihilation cross sections are given by

$$\begin{aligned}\sigma_{XX\rightarrow\tau\tau^*} &= \frac{(\lambda'_{L\tau}{}^2 + \lambda'_{R\tau}{}^2)m_\tau^2}{32\pi(m_{\tilde{Y}^{lep.}}^2 + m_X^2)^2} \sqrt{1 - \frac{m_\tau^2}{m_X^2}} \left[1 + \frac{1}{3} \frac{\vec{p}^2}{m_\tau^2} \right] \\ \sigma_{XX\rightarrow\tilde{f}_i\tilde{f}_i^*} &= \frac{(\lambda'_{Li}{}^2 + \lambda'_{Ri}{}^2)^2}{16\pi} \sqrt{1 - \frac{m_{\tilde{f}_i}^2}{m_X^2} \frac{m_X^2 - m_{\tilde{f}_i}^2}{(m_{\tilde{Y}^{lep.}}^2 + m_X^2 - m_{\tilde{f}_i}^2)^2}},\end{aligned}\quad (10)$$

and the corresponding diagrams are shown in Fig. 2. We set $\lambda'_\tau \equiv \lambda'_{L\tau} = \lambda'_{R\tau}$ and $\lambda'_i \equiv \lambda'_{Li} = \lambda'_{Ri}$.

DM annihilation to squarks requires the squark masses to be lighter than the DM mass, which in turn is lighter than the connector, which is bounded by precision electroweak data and perturbativity to be lighter than 600 GeV. Generally though, in GMSB-inspired models the squarks are heavier than the sleptons due to the hierarchy of the gauge couplings. Thus, such light squark masses are not natural. Besides, the cascade products of heavy squarks and the resulting neutrino spectra are extremely model dependent, being determined by the features of the sparticle spectrum. For these reasons we decide to avoid the treatment of annihilation to squarks and focus on the channels dominated by leptonic Yukawa couplings.

3 Annihilation Products and Propagation

3.1 DM Annihilation in the Sun

The time dependence of the number of DM particles in the Sun is determined by the balance of capture and annihilation. A massive particle can be gravitationally captured by the Sun from the galactic halo at a rate C_\odot . On the other hand, annihilation at the center of the Sun will decrease the number of particles at a rate Γ_A . Thus, the time evolution of the number of DM particles in

the Sun N is given by the solution to the differential equation [22],

$$\frac{dN}{dt} = C_\odot - C_A N^2, \quad (11)$$

where $C_A = 2\Gamma_A/N^2$.

Assuming that the number of collisions DM particles undergo inside the Sun during the Sun's lifetime is large enough for them to thermalize [23], the number density of DM particles at a distance r from the solar core can be expressed in terms of the DM mass m_X , the temperature of the Sun T and the gravitational potential $\phi(r) = 2\pi\rho r^2/(3M_{Pl}^2)$:

$$n(r) = n_0 e^{-\phi(r)\frac{m_X}{T}} = n_0 e^{-\frac{2\pi\rho r^2}{3M_{Pl}^2} \frac{m_X}{T}}, \quad (12)$$

where n_0 is the DM number density at the center of the Sun, ρ is the average density of the Sun and $M_{Pl} = 1.22 \times 10^{19}$ GeV is the Planck mass. C_A is then a constant that depends only on ρ , T and the annihilation cross section $\langle\sigma_{Av}\rangle$ averaged over the velocity distribution in the limit $v \rightarrow 0$:

$$C_A = \frac{\int n(r)^2 \langle\sigma_{Av}\rangle d^3r}{(\int n(r) d^3r)^2} = \langle\sigma_{Av}\rangle \left(\frac{3M_{Pl}^2 T}{m_X \rho}\right)^{-\frac{3}{2}}. \quad (13)$$

Equation (11) admits the solution,

$$N(t) = \sqrt{\frac{C_\odot}{C_A}} \tanh\left(\frac{t}{\tau}\right), \quad (14)$$

where $\tau \equiv 1/\sqrt{C_A C_\odot}$ is the characteristic time necessary to reach equilibrium. For $t \sim 4.5$ Gyr and $\langle\sigma_{ann.v}\rangle \sim 1$ pb (as is the case for WIMPlless dark matter) and $\sigma_{SD} \gtrsim 10^{-6}$ pb (the range of interest for IceCube/DeepCore), it is known [22, 23] that $t/\tau \gg 1$ for the range $150 \text{ GeV} < m_X < 600 \text{ GeV}$ considered here. Since $\Gamma_A = C_A N^2/2 = C_\odot \tanh^2(t/\tau)/2$, one can easily see that when $t \gg \tau$, $\Gamma_A \rightarrow \Gamma_{eq} \equiv C_\odot/2$.

This limit simplifies the calculations, as it relates the event rate to the DM-nucleon scattering cross section, thus bypassing all the astrophysical uncertainties related to the solar model. However, the condition of equilibrium is not guaranteed. For example, in Ref. [24] it was recently shown that there are regions of mSUGRA parameter space for which the annihilation rate is far below the capture rate. Moreover, since DM can annihilate to hidden sector particles as well as MSSM particles, the annihilation rate relevant for neutrino detection is scaled by the branching fraction to MSSM decay products, $\Gamma_A^{MSSM} = \Gamma_A B_F^{MSSM}$. In the figures presented in Sec. 4, we account for these uncertainties by scaling the muon event rates at the detector by the parameter $\xi \equiv \Gamma_A^{MSSM}/\Gamma_{eq} = B_F^{MSSM} \tanh^2(t/\tau)$. However, our discussion assumes $\xi = 1$, as this choice allows us to draw quantitative conclusions. Event rates at conditions away from equilibrium can be obtained by simply choosing a lower value for ξ .

3.2 Capture Rate

If WIMPless DM is Majorana, it has only SD scattering. This property presents the advantage of not being tied to the direct-detection bounds on the SI cross section. The corresponding capture rate is [22, 25],

$$C_{\odot} \simeq 3.35 \times 10^{20} \text{ s}^{-1} \left(\frac{\sigma_{SD}}{10^{-6} \text{ pb}} \right) \left(\frac{100 \text{ GeV}}{m_X} \right)^2, \quad (15)$$

where we have taken the local DM density to be 0.3 GeV/cm^3 , and the root-mean-square of the velocity dispersion in the halo to be 270 km/s . For SD scattering in the Sun, the only relevant nucleus with spin is hydrogen.

3.3 Neutrino Spectra

We limit our consideration to the cases of DM particles annihilating to taus, staus and sneutrinos of all three families. For the cases where DM annihilates to sparticles, we assume that the annihilation product is the next-to-next-to-lightest SUSY particle (NNLSP), and the lightest neutralino is the next-to-lightest SUSY particle (NLSP); in GMSB the lightest SUSY particle (LSP) is the gravitino. Such a choice is consistent with generic sparticle spectra originating from GMSB.

In Figs. 3a, 3b and 3c, we show the neutrino energy spectra dN/dE_{ν} for an annihilation of WIMPless particles of mass $m_X = 150 \text{ GeV}$ into taus, $X\bar{X} \rightarrow \tau^{-}\tau^{+}$. The corresponding antineutrino spectra are shown in Figs. 3d, 3e and 3f. Figures 3a and 3d show the spectra at the origin; Figs. 3b and 3e at the surface of the Sun and Figs. 3c and 3f at the detector. Similar spectra are obtained for annihilation into taus for the other two benchmark DM masses we consider in this paper: $m_X = 300 \text{ GeV}$ and $m_X = 400 \text{ GeV}$. In Fig. 4 we show the neutrino and antineutrino spectra from annihilation into staus ($X\bar{X} \rightarrow \tilde{\tau}_1^{-}\tilde{\tau}_1^{+}$) of a $m_X = 300 \text{ GeV}$ DM particle. In Fig. 5, the neutrino and antineutrino spectra from $m_X = 400 \text{ GeV}$ DM annihilation into $\tilde{\nu}_{eL}\tilde{\nu}_{eL}$, $\tilde{\nu}_{\mu L}\tilde{\nu}_{\mu L}$ and $\tilde{\nu}_{\tau L}\tilde{\nu}_{\tau L}$ with equal branching fractions are shown. The spectral shapes for $m_X = 150, 400 \text{ GeV}$ DM annihilation into staus are similar to those in Fig. 4, while those for $m_X = 150, 300 \text{ GeV}$ DM annihilation into sneutrinos are similar to Fig. 5.

We obtain the neutrino spectra by cascading the annihilation products with PYTHIA 6.4 [26]. In the cases of Figs. 4 and 5 we consider a typical GMSB spectrum, like the one given in Ref. [27]. We assume $m_{\tilde{\tau}_1} = 137 \text{ GeV}$ and $m_{\tilde{Z}_1^0} = 94.5 \text{ GeV}$, corresponding to $\tan\beta \sim 10$. The cascade proceeds primarily through $\tilde{\tau}_1^{-(+)} \rightarrow \tilde{Z}_1^0\tau^{-(+)}$, hence the higher number of ν_{τ} s and $\bar{\nu}_{\tau}$ s at the origin in Figs. 4a and 4d.

In the case where the DM candidate annihilates primarily into sneutrinos (Fig. 5), we assumed for simplicity that the three sneutrino masses are degenerate ($m_{\tilde{\nu}} = 111.5 \text{ GeV}$) and that the couplings to the three flavors are identical, so that the production spectra for the three neutrino

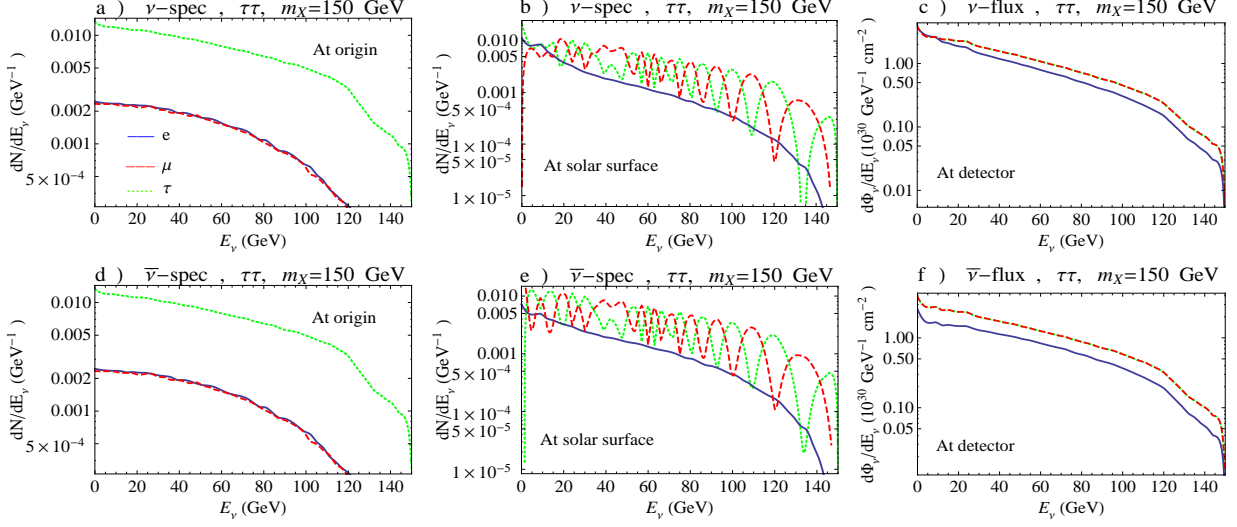


Figure 3: Neutrino spectra and fluxes for all three flavors per $X\bar{X} \rightarrow \tau^-\tau^+$ annihilation with $m_X = 150$ GeV, a) at production, b) at the surface of the Sun, c) flux $\Phi_\nu \equiv N/4\pi R_{SE}^2$ at Earth. d), e), f) $\bar{\nu}$ spectra and fluxes.

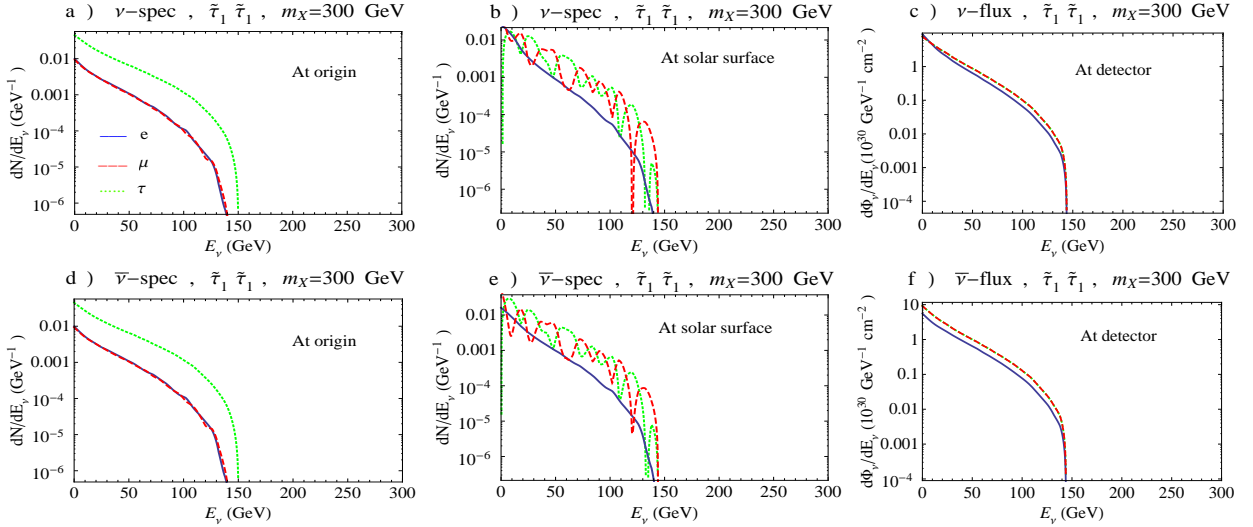


Figure 4: Similar to Fig. 3 for $X\bar{X} \rightarrow \tilde{\tau}_1^-\tilde{\tau}_1^+$ with $m_X = 300$ GeV.

families are the same, $\tilde{\nu}_{eL(\mu L, \tau L)} \rightarrow \tilde{Z}_1^0 \nu_{e(\mu, \tau)}$. As in the previous case we have $m_{\tilde{Z}_1^0} = 94.5$ GeV, corresponding to $\tan\beta \sim 10$. Note that since WIMPLESS DM particles only annihilate leptonically into SM particles or the NNLSP, the neutrino spectra have the same shape whether X is heavier or lighter than the top quark. Notice that the spectra from tau decays are broader than in the stau and sneutrino cases. This is expected because of the influence of the neutralino mass on kinematics. As a matter of fact, the step drop in the neutrino spectra arising from annihilation to sparticles

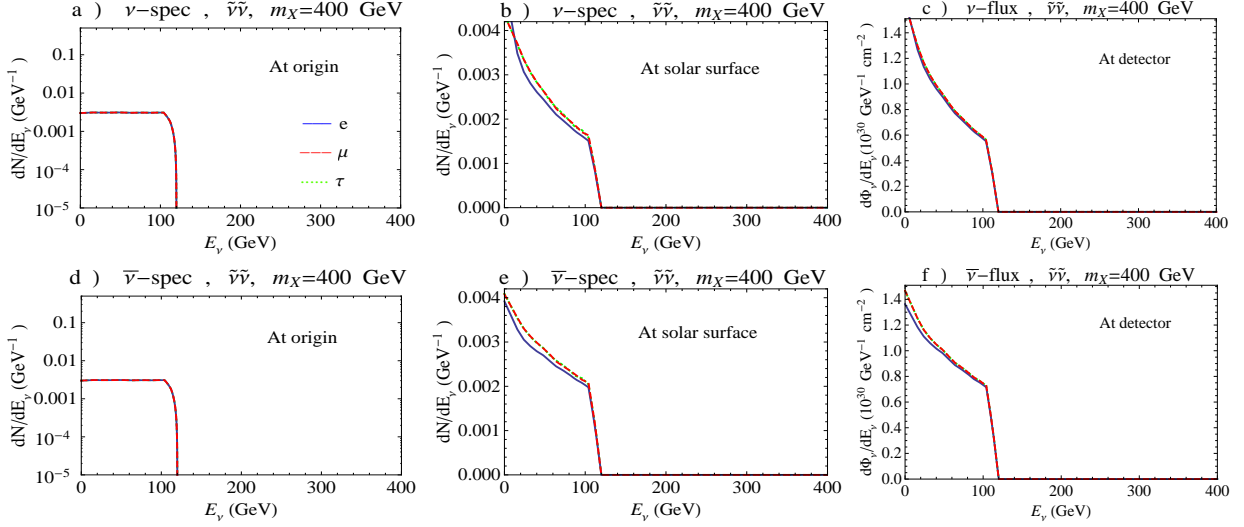


Figure 5: Similar to Figs. 3, 4 for $X\bar{X} \rightarrow \tilde{\nu}_{e(\mu,\tau)}\tilde{\nu}_{e(\mu,\tau)}$ with equal branching fractions and $m_X = 400$ GeV.

will have important consequences for detection at IceCube and DeepCore, as we discuss in Sec. 4.

The propagation of neutrinos produced at the center of the Sun through the solar medium and to the Earth is detailed in the appendices. We take into account neutrino oscillations and the effects of neutral-current (NC) and charged-current (CC) interactions and tau regeneration. In Figs. 3b, 3e and corresponding panels of Figs. 4 and 5 we show the neutrino and antineutrino fluxes after propagation to the surface of the Sun. They present expected features; for example, an accumulation of events at lower energies is visible, due to energy losses of the neutrinos undergoing NC and CC scattering inside the Sun. Tau regeneration, too, has the effect of increasing the low-energy neutrino flux. Furthermore, we see that flavor mixing affects the ν_μ and ν_τ spectra but leaves the ν_e spectra unaltered, since $\theta_{23} = 45^\circ$, $\theta_{13} = 0^\circ$ (Eq. 18 of Appendix A). Figures 3c, 3f and corresponding panels of Figs. 4 and 5 show the fluxes at the Earth after our averaging procedure, described in Appendix A. We define the flux $\Phi_\nu \equiv N/(4\pi R_{SE}^2)$, with $R_{SE} \sim 1$ AU being the Sun-Earth distance. Our results are in very good agreement with those of Ref. [28]. Notice that almost all modulation is washed out.

The flux of high energy neutrinos produced by DM annihilation can be detected by neutrino telescopes like IceCube [29]. The IceCube detector at the South Pole is an array of 80 strings uniformly spaced 125 m from one another, each with 60 digital optical modules. It is deployed at a depth between 1450 m and 2450 m, and the instrumented volume of ice covers 1 km^3 . When muon neutrinos undergo CC scattering on nucleons in ice they produce a muon that propagates through the ice. These muons leave a trail of Cherenkov radiation that can be detected by the optical

modules. We are therefore interested in determining the muon and antimuon flux in and near the detector, taking into account possible energy losses due to the propagation in ice. DeepCore [30], an extension of IceCube, is a denser (72 m spacing) array of six strings surrounding one of the central strings of IceCube, most of them placed below the “dust layer” at a depth of 2100 m. As detailed in Appendix B, DeepCore’s denser strings lower the neutrino energy threshold with respect to IceCube and thus allow detection of neutrinos from annihilation of DM particles of a lower mass. Besides, DeepCore is designed to use the outer instrumented volume of IceCube as a veto on atmospheric muons from above the horizon to a level of one part in 10^6 , thus drastically reducing the background. Such properties make it a perfect instrument to test the WIMPless scenario in the case of Majorana DM.

DeepCore’s muon effective volume becomes insignificant below muon energies of 10 GeV [31]. At energies between 10 and 35 GeV DeepCore cannot provide directional information, since only one or two optical modules will be triggered. Very good directional information is needed to track the Sun throughout the year, so we fix DeepCore’s energy threshold at $E_{min} = 35$ GeV [32]. For IceCube we consider the very optimistic threshold $E_{thr} = 100$ GeV.

4 Results

In this section we investigate the prospects for DM detection at IceCube and DeepCore. We consider a 3σ -detection as

$$\text{“}3\sigma\text{-detection”} \leftrightarrow \frac{N_\mu}{\sqrt{N_{BG}}} = 3, \quad (16)$$

where N_μ is the observed number of muon events and N_{BG} is the number of muon events due to the atmospheric neutrino background [33], which is discussed further in Appendix C.

For the IceCube detector we divide the muon events into *upward* and *contained* events, following the treatment of [34]. As we discuss in Appendix B, the former are due to upward going neutrinos interacting outside the detector volume, the latter to neutrinos that interact within the instrumented volume. To evaluate the event rate we track the Sun in the sky at different times of the year, and consider only events detected when the Sun is below the horizon. The distinction between upward and contained events does not apply to DeepCore, which only sees contained events. For DeepCore, IceCube will veto atmospheric muons from above the horizon to a level of one part in 10^6 . Therefore, at DeepCore we consider the signal detected throughout the year. We consider a period of 5 yrs of observation. As anticipated in Sec. 3, we rescale the event rates obtained at equilibrium by $\xi \equiv \Gamma_A^{MSSM}/\Gamma_{eq}$.

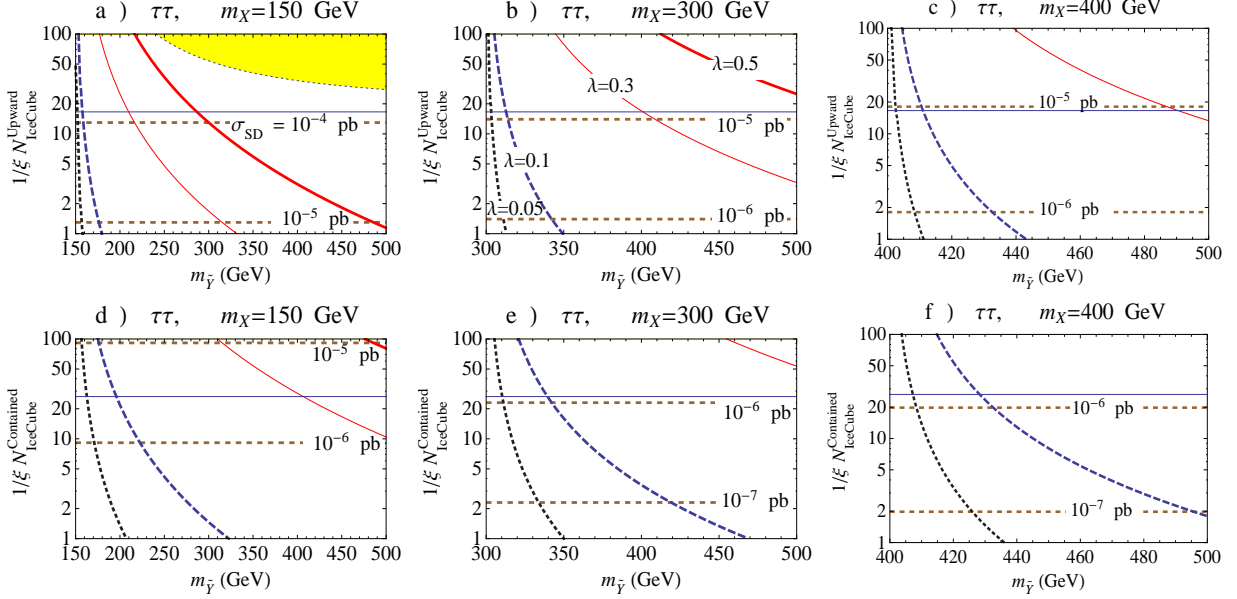


Figure 6: Number of upward and contained events in 5 yrs of observation at IceCube for three values of m_X as a function of $m_{\tilde{\chi}}$ for the $\tau^-\tau^+$ channel for several choices of $\lambda = \lambda_{(L,R)(u,d)}$. Dotted black: $\lambda = 0.05$; dashed blue: $\lambda = 0.1$; solid thin red: $\lambda = 0.3$; solid thick red: $\lambda = 0.5$. The blue horizontal lines represent the number of events needed for a 3σ discovery in 5 yrs of observation. The dashed brown horizontal lines represent σ_{SD} in pb. The yellow band represents values of λ that yield the correct relic abundance.

4.1 Event Rates: Tau channel

In Fig. 6 we plot the upward and contained event rates at IceCube for our three benchmark DM masses for the $XX \rightarrow \tau^-\tau^+$ channel, as a function of the scalar connector mass $m_{\tilde{\chi}}$ and the Yukawa couplings. We assume that the masses of the up-type and down-type squarks \tilde{Y} are degenerate, and that $\lambda \equiv \lambda_{(L,R)(u,d)}$. In Fig. 7 we plot the contained event rates at DeepCore for the same channel. The event rates [see Eqs. (35), (37) and (39) of Appendix B] are evaluated for values of the Yukawa couplings which allow calculations in the perturbative regime. The values in pb of SD cross sections that correspond to the event rates are shown as horizontal dashed brown lines, and labeled on the plots. Notice the following features:

- As we show in Appendix C, the atmospheric background to upward events in IceCube is $N_{BG}^{Up} \simeq 6.1 \text{ yr}^{-1}$, while the background to contained events is $N_{BG}^{Con} \simeq 15.6 \text{ yr}^{-1}$. The background to contained events at DeepCore is $N_{BG}^{DC} \simeq 2.5 \text{ yr}^{-1}$. The blue horizontal lines in Figs. 6 and 7 indicate the number of signal events needed for a 3σ detection in 5 yrs. We see that a 3σ -detection in upward events at IceCube is possible for reasonable values of λ and $m_{\tilde{\chi}}$. The contained event sample offers even better prospects.

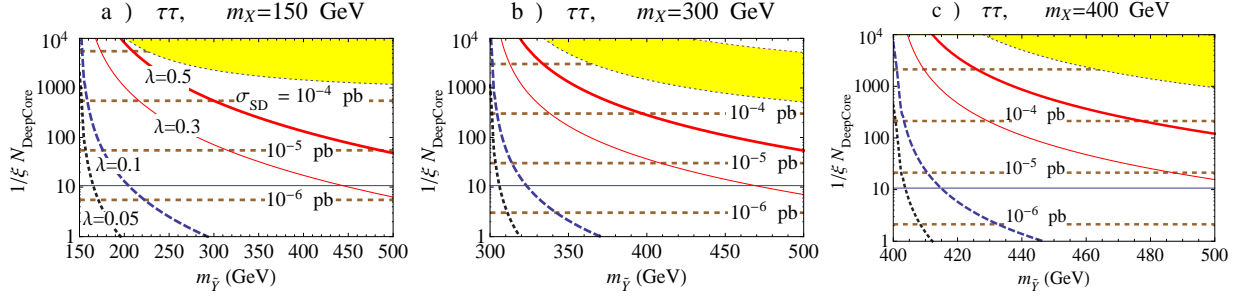


Figure 7: Similar to Fig. 6 for contained events at DeepCore.

- In Fig. 7a we see that DeepCore significantly improves the prospects for observation of events for $m_X = 150$ GeV. A 3σ detection in this channel can be obtained with Yukawa couplings of about 0.3 without a need for resonant enhancement. If the Yukawa couplings are allowed to assume larger values, the prospects for signal detection become even more robust.

- For DM masses well above E_{thr} the advantages of DeepCore in the τ channel are less evident. As a matter of fact a 3σ detection is more likely in the contained events at IceCube. For such high masses the propagator suppression of the SD cross section reduces the flux at the detector and makes the larger $m_{\tilde{\chi}}$ effective volume of IceCube advantageous.

One may ask whether it is possible to relate the size of the Yukawa coupling λ responsible for SD scattering to the size of the Yukawa couplings λ_τ that appear in Eq. (10), and are responsible for the annihilation to SM particles. This is possible under certain assumptions:

- The yellow bands in Figs. 6 and 7 indicate the region with $0.1 \text{ pb} \leq \sigma_{X\bar{X} \rightarrow \tau\bar{\tau}} v \leq 1 \text{ pb}$, assuming $\lambda'_\tau = \lambda$ and $m_{\tilde{\chi}_{lep.}} = m_{\tilde{\chi}}$. For this range of $\sigma_{X\bar{X} \rightarrow \tau\bar{\tau}} v$ (assuming there are light bosons in the hidden sector), annihilation to MSSM particles has a large enough branching fraction to permit observation at neutrino telescopes, while not being so large as to dilute the relic abundance and thwart the WIMPlless miracle. Note however, that this constraint is only relevant if DM annihilation to the hidden sector is not chirality/ p -wave suppressed.

- If $\lambda'_\tau/\lambda > 1$, the yellow band shifts down to lower values. Such a situation may be desirable in the $\tau^-\tau^+$ channel so that the iso- λ curves pass through the yellow bands, i.e., the relic abundance and observable signals at neutrino telescopes can be simultaneously obtained for more of the parameter space.

- As is clear from inspection of Eq. (9) and the first of Eqs. (10), the capture rate depends on λ and $m_{\tilde{\chi}}$ while the annihilation cross section to taus depends on λ'_τ and $m_{\tilde{\chi}_{lep.}}$. ξ depends on the details of the solar model, particularly on the ratio T/ρ in Eq. (13), and on the ratios λ'_τ/λ and $m_{\tilde{\chi}}/m_{\tilde{\chi}_{lep.}}$. A detailed analysis of these aspects is beyond the scope of this paper.

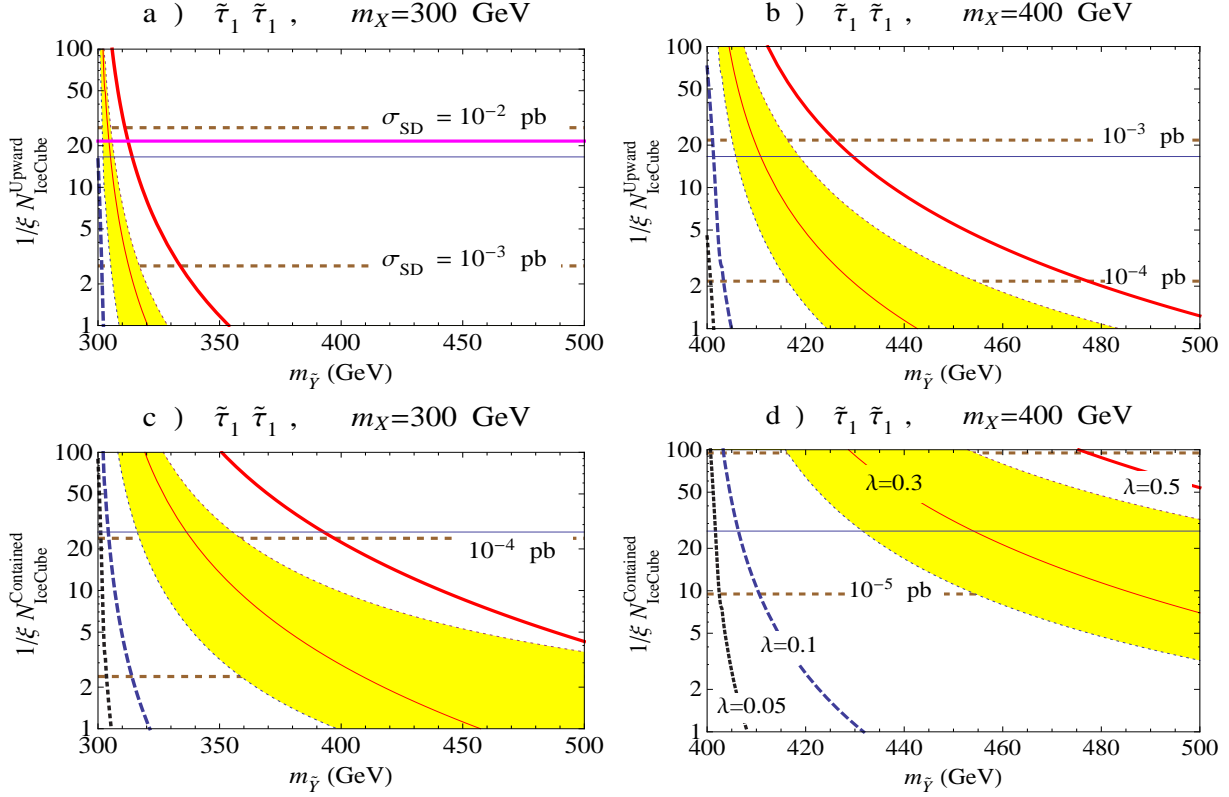


Figure 8: Similar to Fig. 6 for the $\tilde{\tau}_1^- \tilde{\tau}_1^+$ channel. IceCube is insensitive to this channel for $m_X = 150$ GeV. The thick pink horizontal line represents the Super-K 90% C. L. upper bound on σ_{SD} .

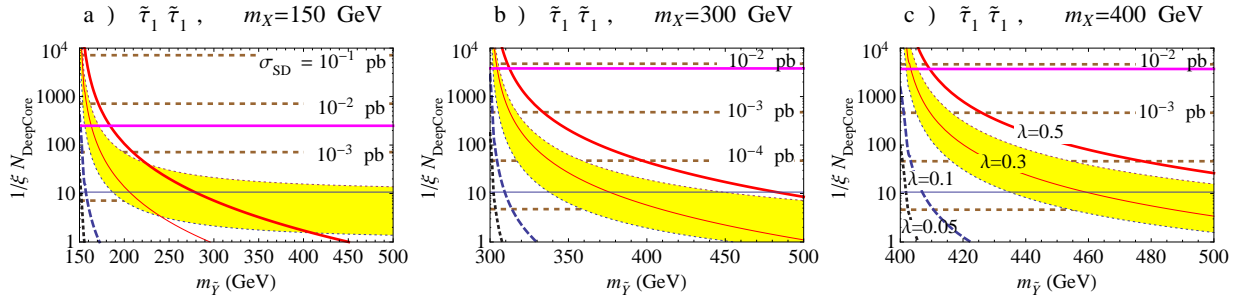


Figure 9: Similar to Fig. 7 for the $\tilde{\tau}_1^- \tilde{\tau}_1^+$ channel. The thick pink horizontal line represents the Super-K 90% C. L. upper bound on σ_{SD} .

4.2 Event Rates: Stau and sneutrino channels

In Figs. 8 and 9 we compare the performances of IceCube and DeepCore, respectively, for the stau channel. Figs. 10 and 11 show our results for the sneutrino channel. The 90% C. L. upper bound placed by Super-Kamiokande [35] on σ_{SD} is indicated on the plots by a thick horizontal

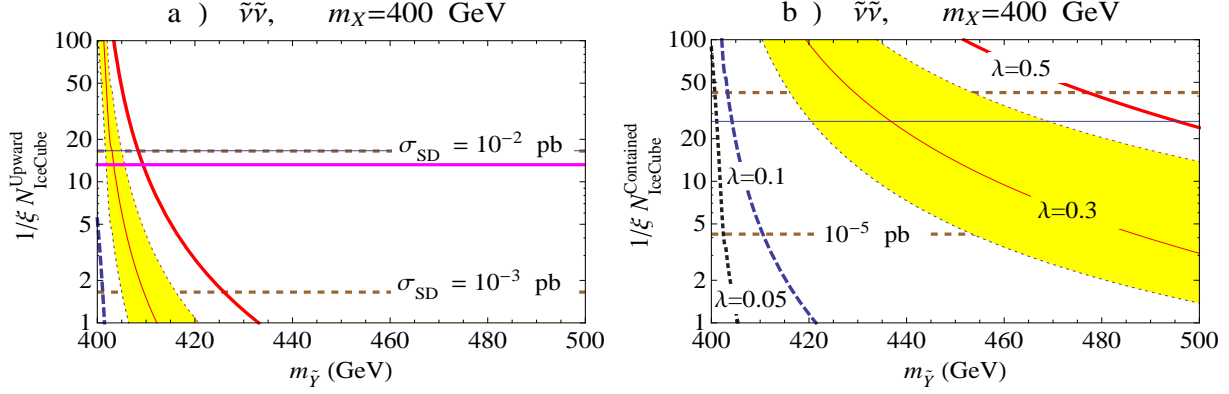


Figure 10: Similar to Fig. 6 for the $\tilde{\nu}\tilde{\nu}$ channel. IceCube is insensitive to this channel for $m_X = 150$ GeV, 300 GeV. The thick pink horizontal line represents the Super-K 90% C. L. upper bound on σ_{SD} . In a), the solid blue horizontal line is coincident with the dashed brown line representing $\sigma_{SD} = 10^{-2}$ pb.

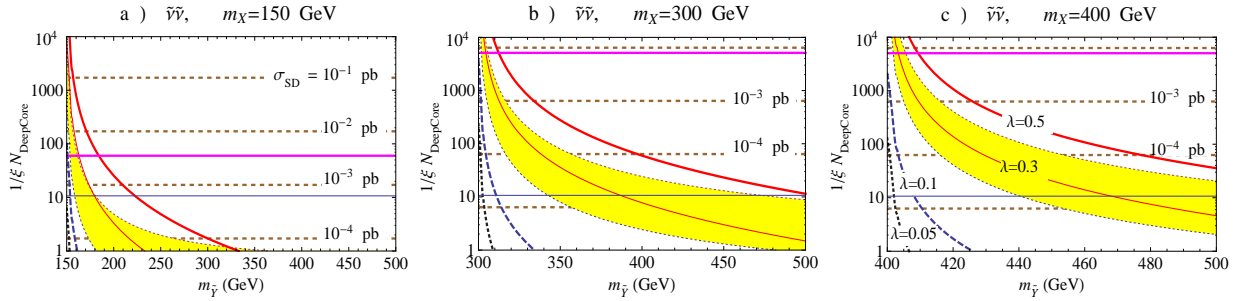


Figure 11: Similar to Fig. 7 for the $\tilde{\nu}\tilde{\nu}$ channel. The thick pink horizontal line represents the Super-K 90% C. L. upper bound on σ_{SD} .

pink line. For $m_X = 150$ GeV this bound is $\sigma_{SD}^{Max} \simeq 3.5 \times 10^{-3}$ pb and for $m_X = 300 - 400$ GeV, $\sigma_{SD}^{Max} \simeq 8 \times 10^{-3}$ pb. For the $\tau^-\tau^+$ channel these bounds are off scale and therefore not visible. The advantages of DeepCore in the observation of neutrino fluxes from low-mass DM are evident:

- For our choice of spectra and energy thresholds, DM particles with a 150 GeV (300 GeV) mass do not produce observable events at IceCube in the two sparticle channels (sneutrino channel). At production, neutrino spectra for annihilation of $m_X = 150$ GeV DM particles become negligible above 60 GeV for the stau channel and above 40 GeV for the sneutrino channel. Neutrino spectra originating from $m_X = 300$ GeV DM annihilation into sneutrinos are negligible above 80 GeV. Thus, with a threshold energy $E_{thr} = 100$ GeV no signal is expected for these channels at IceCube.

- As Fig. 8a shows, even if observation of upward events at IceCube is possible in the stau channel for $m_X = 300$ GeV, the region of parameter space allowed is very narrow. It is represented by the strip between the thin blue and thick pink horizontal lines. Similarly, Fig. 10a shows that a

3σ discovery in upward events for $m_X = 400$ GeV in the sneutrino channel is incompatible with Super-K data, as the thin blue line is above the thick pink line. Figs. 8c and 10b show that, as usual, the contained events offer better detection prospects at IceCube: assuming $\lambda = 0.5$, 3σ detection is obtained with a connector mass within 31% of $m_X = 300$ GeV in the stau channel, and within 24% of $m_X = 400$ GeV in the sneutrino channel.

The performance of DeepCore is much less sensitive to the annihilation channel than IceCube, because the lower energy threshold allows integration of much of the neutrino spectra independent of its shape or features.

- Even for values of m_X that do not allow observation of events at Icecube, DeepCore is able to observe events at 3σ in 5 yrs for reasonable values of λ and $m_{\tilde{\chi}}$. However, the region of parameter space for which DeepCore is sensitive to the $m_X = 150$ GeV sparticle channels is very narrow, as can be seen in Figs. 9a and 11a.

- The advantages of DeepCore over IceCube are not substantial for heavy-DM masses in the stau channel, and the detector fares just a little better in the heavy-DM sneutrino channel. Fig. 9c (11c) shows that 3σ detection of $m_X = 400$ GeV DM in the stau (sneutrino) channel can be obtained with a range of connector masses extended by a mere 3% (18%) with respect to IceCube.

- The yellow bands represent the region of $(m_{\tilde{\chi}}, \lambda)$ -parameter space such that $0.1 \text{ pb} \leq \sigma_{X\bar{X} \rightarrow \tilde{f}_i \tilde{f}_i} v \leq 1 \text{ pb}$, assuming that $\lambda'_i = \lambda$ and $m_{Y^{lep.}} = m_{\tilde{\chi}}$.

It has been recently pointed out [36] that DeepCore should be able to identify contained “cascade” events, which originate from CC interactions of electron and tau neutrinos inside the detector, and from NC interactions of neutrinos of all three flavors. For such events the signal is enhanced with respect to the background at energies $\gtrsim 40$ GeV, since the signal is predominantly due to the CC interactions. Specifically, at such energies the flux of atmospheric ν_μ is from one to a few orders of magnitude larger than the flux of ν_e and ν_τ [37]; thus, ν_μ give the dominant contribution to the background through NC interactions, which are weaker than CC interactions. This could provide an additional method of detection for neutrinos. However, as noted in [29, 38], the angular sensitivity for cascades is $\sim 50^\circ$, which does not permit tracking of the Sun with the desired accuracy. Consequently, we do not consider cascade events as a potential signal.

5 Conclusions

We investigated the prospects for indirect detection of fermion WIMPless DM at IceCube and DeepCore. We considered a hidden sector Majorana DM particle of mass m_X that couples through Yukawa couplings in the superpotential to a connector of mass m_Y and visible sector particles. These models are especially interesting in the context of IceCube/DeepCore because they exhibit

only SD nuclear scattering, for which IceCube/DeepCore is expected to soon provide the greatest experimental sensitivity for $m_X \sim \mathcal{O}(\text{few } 100 \text{ GeV})$.

We focused our attention on DM annihilation to taus, staus and sneutrinos. In order to be captured by the Sun the DM particle needs to couple also to up and down quarks and first generation squarks through the superfield. Annihilation to light fermions does not produce an observable signal because it is chirality suppressed. As for annihilation into squarks, in the GMSB-inspired WIMPless scenario, squarks are generally very heavy and the resulting neutrino spectra are strongly dependent on the features of the sparticle spectrum. Therefore, we assumed that the dominant channels for annihilation are exclusively leptonic. We assumed that if the DM candidate annihilates to SM particles, these are predominantly taus. If it annihilates to supersymmetric particles, these belong to lepton superfields and are the NNLSP, with the lightest neutralino being the NLSP. In the cases of stau and sneutrino annihilation channels we focused our attention on the distinct situations where either the DM candidate couples predominantly to the third family (staus), or it couples with equal strength to degenerate sneutrinos of all three families. We believe this allows us to consider a range of interesting possibilities.

We propagated the neutrino spectra originated by DM annihilation at the center of the Sun through the solar medium. We took into account energy losses due to NC interactions, CC interactions, and tau regeneration. We also implemented neutrino oscillations in the propagation through the Sun.

In order to calculate the event rate at the IceCube detector, we considered upward and contained events, taking into account muon energy losses due to ionization, bremsstrahlung, pair production, and photonuclear effects. The technical details of our analyses are provided in the appendices.

We found that it is not possible to obtain 3σ detection in upward or contained events at IceCube for the stau and sneutrino channel for DM masses $m_X \lesssim 150 \text{ GeV}$ with 5 yrs of data. Moreover, a 300 GeV DM particle would not produce observable events for the sparticle channels, unless the Yukawa couplings are large or the connector mass is not more than about 30% heavier than the DM mass. Indirect detection of these relatively light DM particles is favored in the tau channel, due to the broader neutrino spectra produced in this channel. We quantified the improvement DeepCore brings to the detection prospects in all channels, especially for low m_X . In particular, even in the cases mentioned above, where the steep decrease in flux below the detector energy threshold makes signal detection highly unlikely at IceCube, such limitations do not apply to DeepCore. While the performance of the IceCube detector varies significantly between different channels and different DM masses, thus requiring a case by case analysis, we showed that DeepCore can comfortably produce a 5 yr 3σ detection for any analyzed channel, without strong dependence on the Yukawa couplings or connector masses. We thus find good prospects for probing models of Majorana

fermionic WIMPless DM at IceCube, including the DeepCore extension.

Acknowledgments

We thank A. Erkoca, J. Feng, F. Halzen, I. Mocioiu, B. Morse, M. H. Reno and I. Sarcevic for useful discussions, S. Mrenna and P. Skands for help with Pythia, D. Besson, T. DeYoung, D. Grant, and C. Rott for details about DeepCore/IceCube, and especially Y. Gao for many discussions and inputs. This work was supported by the DoE under Grant Nos. DE-FG02-95ER40896 and DE-FG02-04ER41308, by the NSF under Grant No. PHY-0544278, and by the Wisconsin Alumni Research Foundation.

A Neutrino Propagation

We describe the procedure involving the propagation of neutrinos from the center of the Sun to the Earth, and the detection at IceCube and DeepCore.

Once the neutrinos are produced at the center of the Sun, they need to be propagated through the solar medium, travel to the Earth and be detected at the neutrino telescope. The appropriate formalism involves the density matrix for the neutrino spectra in the flavor basis [39]. We call this ρ , and indicate matrices in boldface.

Neutrinos of energy E_ν can be propagated from a point r to $r + dr$ inside the Sun by solving the Heisenberg equation,

$$\frac{d\rho(E_\nu)}{dr} = -i[\mathbf{H}(E_\nu), \rho(E_\nu)] + \left. \frac{d\rho(E_\nu)}{dr} \right|_{NC} + \left. \frac{d\rho(E_\nu)}{dr} \right|_{CC} + \left. \frac{d\rho(E_\nu)}{dr} \right|_{in}, \quad (17)$$

where \mathbf{H} is the Hamiltonian for neutrino oscillations in matter, the term indicated by in is the injection spectrum at the center of the Sun and the other two terms represent the matter effects due to NC- and CC-interactions. The Hamiltonian is

$$\mathbf{H} = \frac{1}{2E_\nu} \mathbf{U} \text{diag}(0, \Delta m_{21}^2, \Delta m_{31}^2) \mathbf{U}^\dagger + \text{diag}(\sqrt{2}G_F N_e, 0, 0), \quad (18)$$

where \mathbf{U} is the neutrino mixing matrix as given in [40], N_e is the radius-dependent density of electrons inside the Sun, G_F is the Fermi constant, E_ν is the energy of the incoming neutrino, and Δm_{21}^2 and Δm_{31}^2 are the neutrino mass-squared differences, $\Delta m_{ij}^2 = m_i^2 - m_j^2$. We use the following values: $\Delta m_{21}^2 = 8.1 \times 10^{-5} \text{ eV}^2$, $\Delta m_{31}^2 = 2.2 \times 10^{-3} \text{ eV}^2$, $\theta_{12} = 33.2^\circ$, $\theta_{23} = 45^\circ$, $\theta_{13} = 0$. It has been shown in [39, 41] that the oscillation results are not significantly changed if θ_{13} is small but nonzero. The density profile of the Sun is shown in Fig. 12 [42].

The injection term is

$$\left. \frac{d\rho_{ij}}{dr} \right|_{in} (E_\nu) = \delta(r) \delta_{ij} \frac{dN}{dE_\nu}. \quad (19)$$

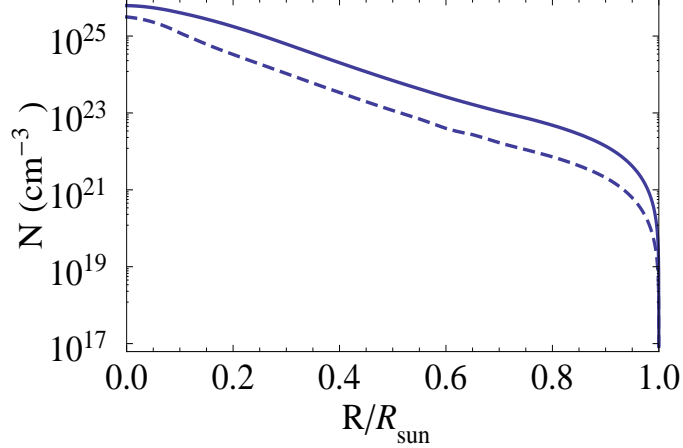


Figure 12: Electron density (solid line) and neutron density (dashed line) as a function of the Sun's radius.

It expresses the number of neutrinos and antineutrinos produced in DM-annihilation at the center of the Sun as a function of energy. It is diagonal in the flavor basis.

In considering the NC and CC terms, we introduce the following quantity which depends on the deep inelastic scattering (DIS) total cross sections σ :

$$\mathbf{\Gamma}_{NC(CC)}(E_\nu, E') = N_p(r)\text{diag}[\sigma(\nu_l p \rightarrow \nu'_l(l) + \text{any})] + N_n(r)\text{diag}[\sigma(\nu_l n \rightarrow \nu'_l(l) + \text{any})], \quad (20)$$

where $N_p(r)(= N_e(r))$ and $N_n(r)$ are the proton and neutron densities inside the Sun, plotted in Fig. 12, E_ν is the incoming neutrino energy, E' the outgoing neutrino (charged lepton) energy and l labels flavor. Then, the neutral-current term is given by

$$\left. \frac{d\rho(E_\nu)}{dr} \right|_{NC} = -\rho(E_\nu) \int_0^{E_\nu} \frac{d\mathbf{\Gamma}_{NC}}{dE'_\nu}(E_\nu, E'_\nu) dE'_\nu + \int_{E_\nu}^{\infty} \frac{d\mathbf{\Gamma}_{NC}}{dE_\nu}(E'_\nu, E_\nu) \rho(E'_\nu) dE'_\nu. \quad (21)$$

The CC term is defined in a similar way but it is more complicated for two reasons. First, the CC-DIS cross sections are not the same for all flavors of neutrinos. As a matter of fact the ν_τ cross sections are suppressed near threshold by the kinematical effects of m_τ . Second, one needs to take into account the effects of tau regeneration that couple the propagation of different flavors (different elements of the density matrix) and elements of the neutrino and antineutrino density matrices.

Tau regeneration is an important effect that leads to a reinjection of the neutrinos produced by the decay of the taus that are CC created by neutrinos of higher energies. The taus produced by energetic neutrinos undergoing CC interactions can decay promptly through various channels, for example, $\tau^- \rightarrow \nu_\tau + \text{any}$, $\tau^- \rightarrow e^- \bar{\nu}_e \nu_\tau$ and $\tau^- \rightarrow \mu^- \bar{\nu}_\mu \nu_\tau$, and similarly for the antiparticles. These processes provide additional sources of energetic neutrinos that reenter the flux with lower energies.

The probabilities of reinjection are encoded in four functions $f_{\nu_\tau \rightarrow \nu_\tau}(u)$, $f_{\bar{\nu}_\tau \rightarrow \bar{\nu}_\tau}(u)$, $f_{\nu_\tau \rightarrow \bar{\nu}_{e,\mu}}(u)$, $f_{\bar{\nu}_\tau \rightarrow \nu_{e,\mu}}(u)$, which depend on the branching ratios of the above channels and on $u \equiv E_\nu^{out}/E_\nu^{in}$, where E_ν^{in} is the energy of the tau neutrino undergoing CC scattering, and E_ν^{out} is the energy of the lower energy neutrinos produced by tau decay [39]. The charged-current contribution to the Heisenberg equation is therefore,

$$\begin{aligned} \left. \frac{d\rho(E_\nu)}{dr} \right|_{CC} &= -\frac{\{\mathbf{\Gamma}_{CC}, \rho\}}{2} + \int_{E_\nu}^{\infty} \frac{dE_\nu^{in}}{E_\nu^{in}} \left[\mathbf{\Pi}_\tau \rho_{\tau\tau}(E_\nu^{in}) \Gamma_{CC}^\tau(E_\nu^{in}) f_{\nu_\tau \rightarrow \nu_\tau} \left(\frac{E_\nu}{E_\nu^{in}} \right) \right. \\ &\quad \left. + \mathbf{\Pi}_{e,\mu} \bar{\rho}_{\tau\tau}(E_\nu^{in}) \bar{\Gamma}_{CC}^\tau(E_\nu^{in}) f_{\bar{\nu}_\tau \rightarrow \nu_{e,\mu}} \left(\frac{E_\nu}{E_\nu^{in}} \right) \right], \end{aligned} \quad (22)$$

$$\begin{aligned} \left. \frac{d\bar{\rho}(E_\nu)}{dr} \right|_{CC} &= -\frac{\{\bar{\mathbf{\Gamma}}_{CC}, \bar{\rho}\}}{2} + \int_{E_\nu}^{\infty} \frac{dE_\nu^{in}}{E_\nu^{in}} \left[\mathbf{\Pi}_\tau \bar{\rho}_{\tau\tau}(E_\nu^{in}) \bar{\Gamma}_{CC}^\tau(E_\nu^{in}) f_{\bar{\nu}_\tau \rightarrow \bar{\nu}_\tau} \left(\frac{E_\nu}{E_\nu^{in}} \right) \right. \\ &\quad \left. + \mathbf{\Pi}_{e,\mu} \rho_{\tau\tau}(E_\nu^{in}) \Gamma_{CC}^\tau(E_\nu^{in}) f_{\nu_\tau \rightarrow \bar{\nu}_{e,\mu}} \left(\frac{E_\nu}{E_\nu^{in}} \right) \right], \end{aligned} \quad (23)$$

where $\mathbf{\Pi}_e = \text{diag}(1, 0, 0)$ are projectors, and similar expressions apply to the other flavors. As is clear from the last term on the right-hand side of Eqs. (22) and (23), tau-regeneration effects couple the two sets of equations. The regeneration probability functions are given by [41],

$$f_{\nu_\tau \rightarrow \nu_\tau}(u) = N \int_u^1 \frac{dz}{z} \left(1 + \frac{z^2}{5} \right) \sum_{i=1}^6 \text{Br}_i \left(g_{0i} \left(\frac{u}{z} \right) - g_{1i} \left(\frac{u}{z} \right) \right), \quad (24)$$

$$f_{\bar{\nu}_\tau \rightarrow \bar{\nu}_\tau}(u) = N \int_u^1 \frac{dz}{z} \left(\frac{1}{5} + z^2 \right) \sum_{i=1}^6 \text{Br}_i \left(g_{0i} \left(\frac{u}{z} \right) - g_{1i} \left(\frac{u}{z} \right) \right), \quad (25)$$

$$f_{\nu_\tau \rightarrow \bar{\nu}_{e,\mu}}(u) = N \int_u^1 \frac{dz}{z} \left(1 + \frac{z^2}{5} \right) 0.18 \left(\tilde{g}_0 \left(\frac{u}{z} \right) - \tilde{g}_1 \left(\frac{u}{z} \right) \right), \quad (26)$$

$$f_{\bar{\nu}_\tau \rightarrow \nu_{e,\mu}}(u) = N \int_u^1 \frac{dz}{z} \left(\frac{1}{5} + z^2 \right) 0.18 \left(\tilde{g}_0 \left(\frac{u}{z} \right) - \tilde{g}_1 \left(\frac{u}{z} \right) \right), \quad (27)$$

where $z = E_\tau/E_\nu^{in}$ and N normalizes the equations so that their integral is either 1 ($\nu_\tau \rightarrow \nu_\tau$ and $\bar{\nu}_\tau \rightarrow \bar{\nu}_\tau$), or 0.18 ($\nu_\tau \rightarrow \bar{\nu}_{e,\mu}$ and $\bar{\nu}_\tau \rightarrow \nu_{e,\mu}$). The functions g_{0i} and g_{1i} are, respectively, the unpolarized and polarized energy spectra of the τ neutrinos originating from the taus in the fragmentation frame, for each final state. The functions \tilde{g}_0 and \tilde{g}_1 are the unpolarized and polarized energy spectra of the $\bar{\nu}_{e,\mu}$ from decay of the τ . The explicit forms of g_{0i} and g_{1i} are given in Table I of [43], and those of \tilde{g}_0 and \tilde{g}_1 are given in Ref. [44]. The branching fractions Br_i refer to the six possible final states: $\tau^- \rightarrow e^- \bar{\nu}_e \nu_\tau$ ($\text{Br}_1 = 0.18$), $\tau^- \rightarrow \mu^- \bar{\nu}_\mu \nu_\tau$ ($\text{Br}_2 = 0.18$), $\tau^- \rightarrow \pi^- \nu_\tau$ ($\text{Br}_3 = 0.12$), $\tau^- \rightarrow a_1 \nu_\tau$ ($\text{Br}_4 = 0.13$), $\tau^- \rightarrow \rho \nu_\tau$ ($\text{Br}_5 = 0.26$), $\tau^- \rightarrow \nu_\tau + \text{any}$ ($\text{Br}_6 = 0.13$).

Once the neutrinos reach the surface of the Sun, the propagation to the Earth is obtained by the following averaging procedure: we rotate the density matrix to the mass basis; drop the off-diagonal terms and rotate it back to the flavor basis. With our choice of neutrino parameters, the averaging should wash out any observable modulation.

B Muon Rates

Upward Events at IceCube

When a muon generated via CC interactions travels through the rock and ice beneath the detector it loses energy due to ionization, bremsstrahlung, pair production, and photonuclear effects [45]. The average energy loss of the muons that travel a distance dz in a medium of density ρ_{med} is given by:

$$\left\langle \frac{dE}{dz} \right\rangle = -(\alpha + \beta(E)E)\rho_{med}(z), \quad (28)$$

where $\alpha = 3.0 \times 10^{-3}$ GeV cm²/g is related to ionization, while $\beta(E)$ takes into account bremsstrahlung, pair production, and photonuclear effects. We take $\beta = 3.0 \times 10^{-6}$ cm²/g and $\rho_{med} = \rho_{ice} = 0.92$ g/cm³. The results from Muon Monte Carlo [46] are reproduced by choosing these values of α and β [47]. Equation (28) can then be easily solved to obtain the final energy $E_{\mu f}$, given initial energy $E_{\mu i}$:

$$E_{\mu f} = -\frac{\alpha}{\beta} + e^{-\beta\rho_{ice}z} \left(E_{\mu i} + \frac{\alpha}{\beta} \right). \quad (29)$$

The average range covered by the muon between energies $E_{\mu i}$, $E_{\mu f}$ is then,

$$R_{\mu}(E_{\mu i}, E_{\mu f}) = \frac{1}{\beta\rho_{ice}} \ln \left(\frac{\alpha + \beta E_{\mu i}}{\alpha + \beta E_{\mu f}} \right). \quad (30)$$

Thus, the muon flux at the detector is obtained by a convolution of the following: the probability of the incoming neutrino to CC scatter with a nucleus in ice; the average range over which energy losses force the muon energy below the detector threshold; the muon probability of surviving its own decay length. This last effect can be parametrized by the survival probability,

$$P_{sur}(E_{\mu i}, E_{\mu f}) = \left[\frac{E_{\mu f}(\alpha + \beta E_{\mu i})}{E_{\mu i}(\alpha + \beta E_{\mu f})} \right]^{\frac{m_{\mu}}{c\tau\alpha\rho_{ice}}}, \quad (31)$$

which is a solution to the differential equation,

$$\frac{dP_{sur}}{dE_{\mu f}} = \frac{P_{sur}}{E_{\mu f}c\tau\rho_{ice}(\alpha + \beta E_{\mu f})/m_{\mu}}, \quad (32)$$

where τ is the muon lifetime and m_{μ} its mass. Folding these effects together gives the spectrum of muon events,

$$\begin{aligned} \frac{d\Phi_{\mu}}{dE_{\mu f}} &= \int_0^{R_{\mu}(m_X, E_{\mu f})} dz e^{\beta\rho_{ice}z} P_{sur}(E_{\mu i}(E_{\mu f}, z), E_{\mu f}) \\ &\times \int_{E_{\mu i}(E_{\mu f}, z)}^{m_X} dE_{\nu} \left[\frac{d\Phi_{\nu}}{dE_{\nu}} \left(\frac{d\sigma_{\nu p}^{CC}}{dE_{\mu i}}(E_{\nu})\rho_p + \frac{d\sigma_{\nu n}^{CC}}{dE_{\mu i}}(E_{\nu})\rho_n \right) \right. \\ &+ \left. \text{(a corresponding contribution for } \bar{\nu}) \right], \end{aligned} \quad (33)$$

where $E_{\mu i}(E_{\mu f}, z)$ is obtained by inverting Eq. (29), $d\sigma^{CC}/dE_{\mu}(E_{\nu})$ are the differential CC-cross sections to protons (νp) and neutrons (νn), $\rho_p \sim 5/9 N_A \text{ cm}^{-3}$ and $\rho_n \sim 4/9 N_A \text{ cm}^{-3}$ are the number densities of nucleons in ice expressed in terms of Avogadro's number N_A , and $d\Phi_{\nu}/dE_{\nu}$ is the neutrino spectrum at Earth, depicted in our specific cases in the third column of Figs. 3, 4 and 5.

The event rate for upward events is obtained by convolving Eq. (33) with the muon *effective area* of the detector, $A_{eff}(E_{\mu f})R(\cos \theta)$, which is constituted by a zenith angle-independent part, shown in Fig. 13a, and a factor $R(\cos \theta) = 0.92 - 0.45 \cos \theta$ that accounts for the rock bed beneath the ice [48]. We take the average of the effective area over the time of the year that the Sun spends below the horizon, namely between the March and September equinoxes. We define the zenith angle θ_z at the South Pole to be the angle centered at the detector with $\theta_z = 0^\circ$ indicating the vertical direction in the sky. θ_z can be parametrized in terms of the time of the year f_y (where $f_y = 0, 1/2$ correspond to the March and September equinoxes, respectively), and the tilt of the Earth axis with respect to the perpendicular to the ecliptic plane, $\theta_t = 23^\circ 26'$:

$$\theta_z(f_y) = \frac{\pi}{2} + \theta_t \sin(2\pi f_y). \quad (34)$$

The event rate reads,

$$N_{events}^{Up} = \xi \Gamma_{eq} \int_0^{m_x} \frac{d\Phi_{\mu}}{dE_{\mu f}} \langle A_{eff}(E_{\mu f})R(\cos \theta_z) \rangle dE_{\mu f}, \quad (35)$$

where ξ and Γ_{eq} are the quantities introduced in Sec. 3.1. $\langle A_{eff}(E_{\mu f})R(\cos \theta_z) \rangle$ is the average over the portion of the solid angle (θ_z, ϕ) that corresponds to the time the Sun spends below the horizon.

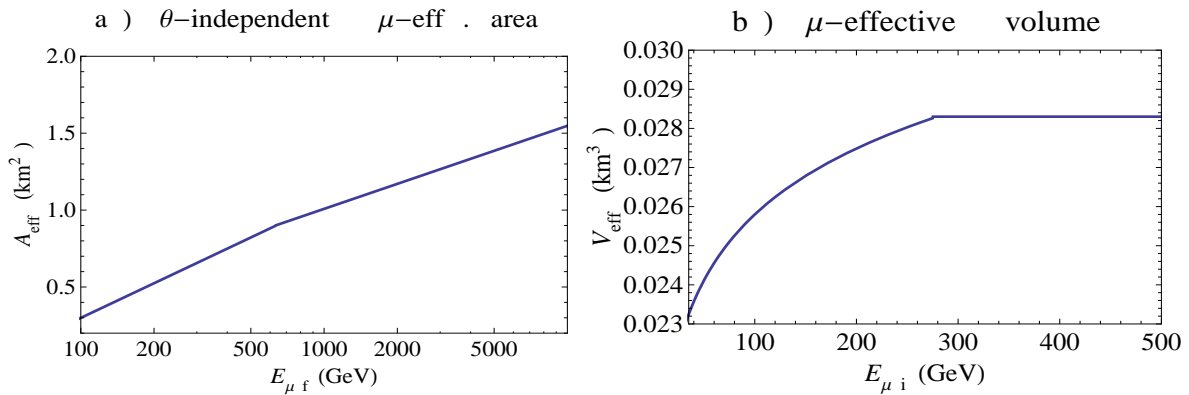


Figure 13: a) The IceCube muon effective area with zenith angle dependence factored out. b) Muon effective volume for DeepCore.

Contained Events at IceCube

For neutrinos that interact within the detector volume, the resulting muons do not lose an appreciable fraction of their energies. Following notation similar to the previous subsection (except that we identify $E_\mu \equiv E_{\mu i}$ since the muons do not propagate) the muon flux for contained events is given by

$$\frac{d\Phi_\mu}{dE_\mu} = L \int_{E_\mu}^{m_x} dE_\nu \left[\frac{d\Phi_\nu}{dE_\nu} \left(\frac{d\sigma_{\nu p}^{CC}}{dE_\mu}(E_\nu)\rho_p + \frac{d\sigma_{\nu n}^{CC}}{dE_\mu}(E_\nu)\rho_n \right) + (\nu \rightarrow \bar{\nu}) \right], \quad (36)$$

where $L \sim 1$ km is the size of the IceCube detector. The event rate reads

$$N_{events}^C = \xi \Gamma_{eq} \int_{E_{thr}}^{m_x} \frac{d\Phi_\mu}{dE_\mu} (1 \text{ km}^2) dE_\mu, \quad (37)$$

where $E_{thr} = 100$ GeV is the energy threshold of the IceCube detector. As mentioned above, we only consider events observed between the March and September equinoxes.

Events at DeepCore

The great advantage of DeepCore with respect to IceCube is that the outer instrumented volume of IceCube will serve as a veto to atmospheric muon events up to one part in 10^6 [29], so that data can be collected throughout the year, i.e., even when the Sun is above the horizon. The rate for contained events at DeepCore can be calculated by convolving Eq. (36) with the muon *effective volume* $V_{eff}(E_{\mu i})$. In the most optimistic estimates the effective volume is constant for muon energies above ~ 300 GeV, and drops significantly at lower energies [31]. As explained in Sec. 3.3, for DeepCore we consider the interval $E_{\mu i} > E_{min} = 35$ GeV. We find that in this interval the effective volume in km^3 can be parametrized by

$$V_{eff}(E_{\mu i}) = (0.0056 \log E_{\mu i} + 0.0146)\Theta(275 - E_{\mu i}) + 0.0283\Theta(E_{\mu i} - 275), \quad (38)$$

where Θ is the Heaviside step function and $E_{\mu i}$ is in GeV. The effective volume is plotted in Fig. 13b.

After convolution one gets

$$N_{events}^{DC} = \xi \Gamma_{eq} \int_{E_{min}}^{m_x} \frac{1}{L} \frac{d\Phi_\mu}{dE_\mu} V_{eff}(E_\mu) dE_\mu. \quad (39)$$

C Atmospheric Background

The angle-dependent flux of atmospheric neutrinos $d\Phi_\nu^{atm}/(dE_\nu d\cos\theta)$ is given in [33]. These neutrinos interact with the medium surrounding the detector and produce muons that constitute the background. As in the case of neutrinos from annihilation, the atmospheric background can be divided in upward and contained events.

By following the notation introduced in the previous subsections we can write the angular dependence of the upward background flux for IceCube as

$$\begin{aligned}
\frac{d\Phi_{\mu}^{atm}}{dE_{\mu f} d \cos \theta_z(f_y)} &= \int_0^{R_{\mu}(E_{Max}, E_{\mu f})} dz e^{\beta \rho_{ice} z} P_{sur}(E_i(E_{\mu f}, z), E_{\mu f}) \\
&\times \int_{E_i(E_{\mu f}, z)}^{E_{Max}} dE_{\nu} \left[\frac{d\Phi_{\nu}^{atm}}{dE_{\nu} d \cos \theta_z(f_y)} \left(\frac{d\sigma_{\nu p}^{CC}}{dE_i}(E_{\nu}) \rho_p + \frac{d\sigma_{\nu n}^{CC}}{dE_i}(E_{\nu}) \rho_n \right) \right. \\
&+ \left. (\nu \rightarrow \bar{\nu}) \right], \tag{40}
\end{aligned}$$

where $E_{Max} \sim 10^4$ GeV is the maximum energy above which the rapidly falling atmospheric flux becomes negligible. The angle-dependent flux, Eq. (40), is integrated over a cone of solid angle $d\Omega = \pi(d\theta)^2$, where the opening angle (half the apex angle) $d\theta \sim 1^\circ$, consistent with the IceCube angular sensitivity [29, 34]. The cone tracks the Sun according to Eq. (34), for the fraction of the year over which the Sun is below the horizon. The number of upward background events for IceCube can be calculated by folding in the effective area $A_{eff}(E_{\mu f})R(\cos \theta_z)$. We find $N_{BG}^{Up} \simeq 6.1 \text{ yr}^{-1}$ where, again, data is taken only between the March and September Equinoxes.

Contained events are those obtained by muon neutrinos undergoing charged-current interactions within the detector volume, thus the angular dependence of the flux is given by

$$\begin{aligned}
\frac{d\Phi_{\mu}^{atm}}{dE_{\mu} d \cos \theta_z(f_y)} &= L \int_{E_{\mu}}^{E_{Max}} dE_{\nu} \left(\rho_p \frac{d\sigma_{\nu}^p(E_{\nu}, E_{\mu})}{dE_{\mu}} + \rho_n \frac{d\sigma_{\nu}^n(E_{\nu}, E_{\mu})}{dE_{\mu}} \right) \frac{d\Phi_{\nu}^{atm}}{dE_{\nu} d \cos \theta_z(f_y)} \\
&+ (\nu \rightarrow \bar{\nu}). \tag{41}
\end{aligned}$$

The number of contained background events in a cone of 1° opening for time of exposure limited to the period between March and September is obtained, as in Eq. (37), by convolving with a constant 1 km^2 area. We get $N_{BG}^{Con} \simeq 15.6 \text{ yr}^{-1}$.

The number of background events for DeepCore over the whole year, obtained by convolving with $V_{eff}(E_{\mu i})/L$, is $N_{BG}^{DC} \simeq 2.5 \text{ yr}^{-1}$.

In Fig. 14 we show the dependence of N_{BG}^{Up} , N_{BG}^{Con} and N_{BG}^{DC} on the opening angle $d\theta$. The thin blue horizontal lines shown in Figs. 6-11 represent the 5 yr 3σ -discovery reach for $d\theta = 1^\circ$. While the angular resolution is expected to be best for directions close to the horizon (and the Sun does not stray more than $23^\circ 26'$ from the horizon at the South Pole), in case the angular resolution of the IceCube and DeepCore detectors do not meet expectations, the background event rates can be obtained from Fig. 14. Then, for a 3σ detection, $N_{\mu} = 3\sqrt{N_{BG}}$ can be trivially recalculated.

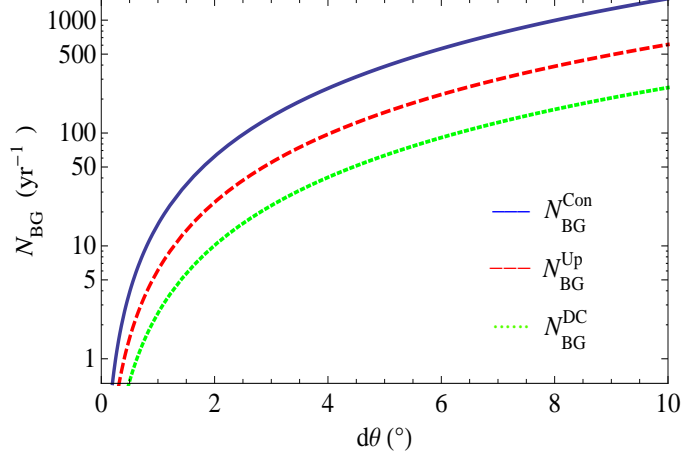


Figure 14: Number of background events per year as a function of the opening angle $d\theta$.

References

- [1] G. Wikstrom and J. Edsjo, JCAP **0904**, 009 (2009) [arXiv:0903.2986 [astro-ph.CO]].
- [2] D. Hooper, F. Petriello, K. M. Zurek and M. Kamionkowski, Phys. Rev. D **79**, 015010 (2009) [arXiv:0808.2464 [hep-ph]]; J. L. Feng, J. Kumar, J. Learned and L. E. Strigari, arXiv:0808.4151 [hep-ph]; J. Kumar, J. G. Learned and S. Smith, Phys. Rev. D **80**, 113002 (2009) [arXiv:0908.1768 [hep-ph]]; V. Niro, A. Bottino, N. Fornengo and S. Scopel, Phys. Rev. D **80**, 095019 (2009) [arXiv:0909.2348 [hep-ph]].
- [3] A. Bottino, F. Donato, N. Fornengo and S. Scopel, Phys. Rev. D **69**, 037302 (2004) [arXiv:hep-ph/0307303]; P. Gondolo and G. Gelmini, Phys. Rev. D **71**, 123520 (2005) [arXiv:hep-ph/0504010]; R. Bernabei *et al.*, Eur. Phys. J. C **53**, 205 (2008) [arXiv:0710.0288 [astro-ph]]; F. Petriello and K. M. Zurek, JHEP **0809**, 047 (2008) [arXiv:0806.3989 [hep-ph]]; A. Bottino, F. Donato, N. Fornengo and S. Scopel, Phys. Rev. D **78**, 083520 (2008) [arXiv:0806.4099 [hep-ph]]. S. Chang, A. Pierce and N. Weiner, arXiv:0808.0196 [hep-ph]; C. Savage, G. Gelmini, P. Gondolo and K. Freese, JCAP **0904**, 010 (2009) [arXiv:0808.3607 [astro-ph]].
- [4] M. Fairbairn and T. Schwetz, JCAP **0901**, 037 (2009) [arXiv:0808.0704 [hep-ph]].
- [5] Z. Ahmed *et al.* [The CDMS-II Collaboration], arXiv:0912.3592 [astro-ph.CO].
- [6] C. E. Aalseth *et al.* [CoGeNT Collaboration], arXiv:1002.4703 [astro-ph.CO].

- [7] A. Bottino, F. Donato, N. Fornengo and S. Scopel, arXiv:0912.4025 [hep-ph]; A. L. Fitzpatrick, D. Hooper and K. M. Zurek, arXiv:1003.0014 [hep-ph]; D. Feldman, Z. Liu and P. Nath, arXiv:1003.0437 [hep-ph]; E. Kuflik, A. Pierce and K. M. Zurek, arXiv:1003.0682 [hep-ph].
- [8] G. Bertone, D. G. Cerdeno, J. I. Collar and B. C. Odom, Phys. Rev. Lett. **99**, 151301 (2007) [arXiv:0705.2502 [astro-ph]]; V. Barger, W. Y. Keung and G. Shaughnessy, Phys. Rev. D **78**, 056007 (2008) [arXiv:0806.1962 [hep-ph]]; G. Belanger, E. Nezri and A. Pukhov, Phys. Rev. D **79**, 015008 (2009) [arXiv:0810.1362 [hep-ph]]; T. Cohen, D. J. Phalen and A. Pierce, arXiv:1001.3408 [hep-ph]; P. Agrawal, Z. Chacko, C. Kilic and R. K. Mishra, arXiv:1003.1912 [hep-ph]; P. Agrawal, Z. Chacko, C. Kilic and R. K. Mishra, arXiv:1003.5905 [hep-ph].
- [9] J. Braun and D. Hubert for the IceCube Collaboration, arXiv:0906.1615 [astro-ph.HE].
- [10] E. Aprile *et al.* [XENON100 Collaboration], arXiv:1005.0380 [astro-ph.CO].
- [11] J. L. Feng and J. Kumar, Phys. Rev. Lett. **101**, 231301 (2008) [arXiv:0803.4196 [hep-ph]].
- [12] J. L. Feng, J. Kumar and L. E. Strigari, Phys. Lett. B **670**, 37 (2008) [arXiv:0806.3746 [hep-ph]]; J. L. Feng, H. Tu and H. B. Yu, JCAP **0810**, 043 (2008) [arXiv:0808.2318 [hep-ph]].
- [13] M. Dine and A. E. Nelson, Phys. Rev. D **48**, 1277 (1993) [arXiv:hep-ph/9303230]; M. Dine, A. E. Nelson, Y. Nir and Y. Shirman, Phys. Rev. D **53**, 2658 (1996) [arXiv:hep-ph/9507378].
- [14] Ya. B. Zeldovich, Adv. Astron. Astrophys. **3**, 241 (1965); H.Y. Chiu, Phys. Rev. Lett. **17**, 712 (1966); G. Steigman, Ann. Rev. Nucl. Part. Sci. **29**, 313 (1979); R.J. Scherrer and M.S. Turner, Phys. Rev. D **33**, 1585 (1986).
- [15] H. J. He, N. Polonsky and S. f. Su, Phys. Rev. D **64**, 053004 (2001) [arXiv:hep-ph/0102144]; J. Alwall *et al.*, Eur. Phys. J. C **49**, 791 (2007) [arXiv:hep-ph/0607115]; G. D. Kribs, T. Plehn, M. Spannowsky and T. M. P. Tait, Phys. Rev. D **76**, 075016 (2007) [arXiv:0706.3718 [hep-ph]]; R. Fok and G. D. Kribs, Phys. Rev. D **78**, 075023 (2008) [arXiv:0803.4207 [hep-ph]]; B. Holdom, W. S. Hou, T. Hurth, M. L. Mangano, S. Sultansoy and G. Unel, PMC Phys. A **3**, 4 (2009) [arXiv:0904.4698 [hep-ph]]; M. Hashimoto, arXiv:1001.4335 [hep-ph].
- [16] V. M. Abazov *et al.* [D0 Collaboration], Phys. Rev. Lett. **97**, 171806 (2006) [arXiv:hep-ex/0608013]; T. Aaltonen *et al.* [CDF Collaboration], Phys. Rev. D **76**, 072010 (2007) [arXiv:0707.2567 [hep-ex]].
- [17] J. Alwall, J. L. Feng, J. Kumar and S. Su, arXiv:1002.3366 [hep-ph].
- [18] T. Aaltonen *et al.* [The CDF Collaboration], arXiv:0912.4691 [hep-ex].

- [19] G. K. Mallot, in *Proc. of the 19th Intl. Symp. on Photon and Lepton Interactions at High Energy (LP99), 9-14 August 1999, Stanford, California*, edited by J.A. Jaros and M.E. Peskin (World Scientific, Singapore, 2000), pp 521-537 [arXiv:hep-ex/9912040].
- [20] J. R. Ellis, K. A. Olive and C. Savage, *Phys. Rev. D* **77**, 065026 (2008) [arXiv:0801.3656 [hep-ph]].
- [21] M. A. Shifman, A. I. Vainshtein and V. I. Zakharov, *Phys. Lett. B* **78**, 443 (1978).
- [22] G. Jungman, M. Kamionkowski and K. Griest, *Phys. Rept.* **267**, 195 (1996) [arXiv:hep-ph/9506380].
- [23] K. Griest and D. Seckel, *Nucl. Phys. B* **283**, 681 (1987) [Erratum-ibid. B **296**, 1034 (1988)].
- [24] J. Ellis, K. A. Olive, C. Savage and V. C. Spanos, arXiv:0912.3137 [hep-ph].
- [25] A. Gould, *Astrophys. J.* **321**, 571 (1987); *Astrophys. J.* **388**, 338 (1992).
- [26] T. Sjostrand, S. Mrenna and P. Z. Skands, *JHEP* **0605**, 026 (2006) [arXiv:hep-ph/0603175].
- [27] S. Dimopoulos, S. D. Thomas and J. D. Wells, *Nucl. Phys. B* **488**, 39 (1997) [arXiv:hep-ph/9609434].
- [28] M. Blennow, J. Edsjo and T. Ohlsson, *JCAP* **0801**, 021 (2008) [arXiv:0709.3898 [hep-ph]].
- [29] E. Resconi [IceCube Collaboration], *Nucl. Instrum. Meth. A* **602**, 7 (2009) [arXiv:0807.3891 [astro-ph]].
- [30] O. Schulz [IceCube Collaboration], *AIP Conf. Proc.* **1085**, 783 (2009).
- [31] T. DeYoung, private communication.
- [32] D. Grant, private communication.
- [33] M. Honda, T. Kajita, K. Kasahara, S. Midorikawa and T. Sanuki, *Phys. Rev. D* **75**, 043006 (2007) [arXiv:astro-ph/0611418].
- [34] A. E. Erkoca, M. H. Reno and I. Sarcevic, *Phys. Rev. D* **80**, 043514 (2009) [arXiv:0906.4364 [hep-ph]].
- [35] S. Desai *et al.* [Super-Kamiokande Collaboration], *Phys. Rev. D* **70**, 083523 (2004) [Erratum-ibid. D **70**, 109901 (2004)] [arXiv:hep-ex/0404025].
- [36] S. K. Mandal, M. R. Buckley, K. Freese, D. Spolyar and H. Murayama, *Phys. Rev. D* **81**, 043508 (2010) [arXiv:0911.5188 [hep-ph]].

- [37] T. Stanev, Phys. Rev. Lett. **83**, 5427 (1999) [arXiv:astro-ph/9907018].
- [38] E. Middell, J. McCartin and M. D’Agostino [IceCube Collaboration], in the proceedings of The 31st International Cosmic Ray Conference (ICRC 2009), 7-15 July 2009, Lodz, Poland, 2009.
- [39] M. Cirelli, N. Fornengo, T. Montaruli, I. Sokalski, A. Strumia and F. Vissani, Nucl. Phys. B **727**, 99 (2005) [Erratum-ibid. B **790**, 338 (2008)] [arXiv:hep-ph/0506298].
- [40] C. Amsler *et al.* [Particle Data Group], Phys. Lett. B **667**, 1 (2008).
- [41] V. Barger, W. Y. Keung, G. Shaughnessy and A. Tregre, Phys. Rev. D **76**, 095008 (2007) [arXiv:0708.1325 [hep-ph]].
- [42] J. N. Bahcall, M. H. Pinsonneault and S. Basu, Astrophys. J. **555**, 990 (2001) [arXiv:astro-ph/0010346].
- [43] S. I. Dutta, M. H. Reno and I. Sarcevic, Phys. Rev. D **62**, 123001 (2000) [arXiv:hep-ph/0005310].
- [44] P. Lipari, Astropart. Phys. **1**, 195 (1993).
- [45] P. Lipari and T. Stanev, Phys. Rev. D **44**, 3543 (1991).
- [46] D. Chirkin and W. Rhode, arXiv:hep-ph/0407075.
- [47] Y. Gao, private communication.
- [48] M. C. Gonzalez-Garcia, F. Halzen and S. Mohapatra, Astropart. Phys. **31**, 437 (2009) [arXiv:0902.1176 [astro-ph.HE]].